Cellular metabolism in high-throughput *in vitro* reporter gene assays and implications for the quantitative *in vitro-in vivo* extrapolation

Fabian C. Fischer[1,#], Cedric Abele[1], Luise Henneberger[1], Nils Klüver[2], Maria König[1], Marie Mühlenbrink[1], Rita Schlichting[1], Beate I. Escher[1,3,]*

[1] Helmholtz Centre for Environmental Research - UFZ, Department Cell Toxicology, Permoserstraße 15, 04318 Leipzig, Germany

[2] Helmholtz Centre for Environmental Research - UFZ, Department Bioanalytical Ecotoxicology, Permoserstraße 15, 04318 Leipzig, Germany

[3] Eberhard Karls University Tübingen, Centre for Applied Geoscience, 72074 Tübingen, Germany

[#]Present address: National Institute for Environmental Studies (NIES), Center for Health and Environmental Risk Research, Onogawa 16-2, 305-8506 Tsukuba, Ibaraki, Japan.

*Address correspondence to: beate.escher@ufz.de

Abstract

High-throughput *in vitro* reporter gene assays are increasingly applied to assess the potency of chemicals to alter specific cellular signaling pathways. Genetically modified reporter gene cell lines provide stable readouts of the activation of cellular receptors or transcription factors of interest, but such reporter gene assays have been criticized for not capturing cellular metabolism. We characterized the metabolic activity of the widely applied AREc32 (human breast cancer MCF-7), ARE-bla (human liver cancer HepG2), and GR-bla (human embryonic kidney HEK293) reporter gene cells in absence and in presence of benzo(a)pyrene (BaP), an AhR ligand known to upregulate cytochrome P450 *in vitro* and *in vivo*. We combined fluorescence microscopy with chemical analysis, real-time PCR, and EROD activity measurements to track temporal changes in BaP and its metabolites in the cells and surrounding medium over time in relation to the expression and activity of metabolic enzymes. Decreasing BaP concentrations and formation of metabolites agreed with the high basal CYP1 activity of ARE-bla and the strong *CYP1A1* mRNA induction in AREc32, whereas BaP concentrations were constant in GR-bla, in which neither metabolites nor CYP1 induction were detected. The study emphasizes that differences in sensitivity between reporter gene assays may be caused not only by different reporter constructs but also by a varying biotransformation rate of the evaluated parent chemical. The basal metabolic capacity of reporter gene cells in absence of chemicals is not a clear indication because we demonstrated that the metabolic activity can be upregulated by AhR ligands during the assay. The combination of methods presented here is suitable to characterize the metabolic activity of cells *in vitro* and can improve the interpretation of *in vitro* reporter gene effect data and extrapolation to *in vivo* human exposure.

TOC Art

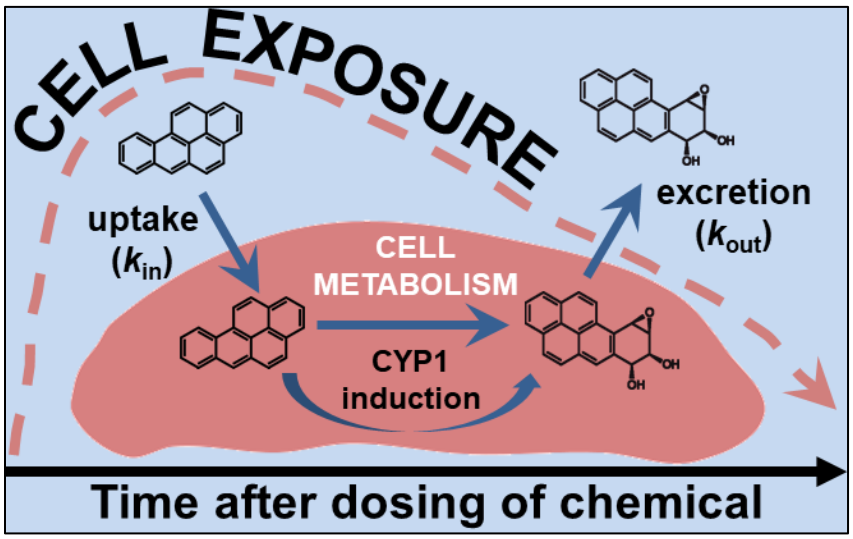
CELL EXPOSURE
uptake
(k_{in})
CELL
METABOLISM
CYP1
induction
excretion
(k_{out})
Time after dosing of chemical

1. Introduction

In vitro cell-based reporter gene assays are gaining increasing attention in human health risk assessment of chemicals. Their implementation in high-throughput screening (HTS) format will contribute to cover the high demand on chemical effect assessment associated with the increasing number and variety of manufactured chemicals. In these artificial cell constructs, a specific receptor-chemical interaction or stress-response pathway is monitored using a reporter gene coupled to the response element of the target receptor (e.g., luciferase or ß-lactamase). This mechanistic approach provides deeper insight in the mode of toxic action (MoA) of a chemical than a standard *in vivo* toxicity test for chemical risk assessment. A large battery of *in vitro* reporter gene assays has been already developed, standardized and miniaturized in multi-well plates for HTS.[1]

One of the biggest systematic screening approaches hitherto is the Toxicology Testing in the 21st Century (Tox21) program that involved the assessment of 10,000 chemicals in 64 quantitative high-throughput reporter gene assays (https://tripod.nih.gov/tox21/assays/). Interestingly, only 14 cell lines form the basis for the reporter gene assays used in Tox21 with different reporter genes implemented into the same cell lines, most abundantly in the human embryonic kidney and liver cancer cell lines HEK293 (42%) and HepG2 (14%). For example, chemical interaction with the androgen receptor (AR) and glucocorticoid receptor (GR) are evaluated in different reporter gene assays and both are based on HEK293 cells.[2] No specific attention was given to biotransformation of the chemical by cellular metabolism in the development of the reporter gene assays.

Metabolism of xenobiotic chemicals usually involves the addition of polar functional groups to the chemicals for facilitated excretion. These biotransformation processes alter the physicochemical properties of the parent chemicals and its potency to affect signaling pathways *in vivo*. The biotransformation of chemicals in *in vitro* reporter gene assays can increase or decrease the apparent activity depending on the biological activity of the metabolites relative to their parent chemical. For example, benzo(a)pyrene (BaP) can be bioactivated through oxidation by cytochrome P450 enzymes into the carcinogenic metabolite benzo(a)pyrene-7,8-diol-9,10-epoxid (BaP-epoxide).[3,4] Higher activities of hydroxylated metabolites were measured in MCF-7 estrogen receptor gene assays compared to the parent BaP,[5] while contrarily lower estrogenic activities were reported for mycotoxins after biotransformation.[6]

55 The cytochrome P450 1A1 enzyme (CYP1A1) is present in all mammalian tissue and plays a key
56 role in metabolism of xenobiotic chemicals by accounting for more than 75% of total metabolism.[7-
57 8] *CYP1A1* gene induction is predominantly mediated by the aryl hydrocarbon (AhR) and cellular
58 tumor antigen receptors (p53) which enter the nucleus upon binding of a chemical and bind to the
59 xenobiotic receptor element (XRE), inducing the *CYP1A1* mRNA expression.[9, 10] The induction of
60 *CYP* genes in *in vitro* cells by chemical exposure was thoroughly investigated in previous studies,[11]
61 amongst others for the native HepG2 and HEK293 cells that are implemented in the ARE-bla and
62 GR-bla Tox21 reporter gene assays.[12-14] For micronucleus frequency *in vitro* assays, a natural
63 biomarker for DNA damage, it has been shown that the sensitivity of the measurement endpoint
64 strongly depends on the metabolic capability of the applied cell line (MCL-5, TK6, and HepG2
65 cells) to form more toxic metabolites.[15] Such case studies indicated the importance of metabolism
66 in 2D cell assays monitoring specific cellular endpoints that are not directly related to their
67 metabolic activity.
68 The biotransformation of test chemical(s) by metabolism is generally not considered in the
69 evaluation of *in vitro* effect data of reporter gene assays but can represent a significant source of
70 uncertainty. Characterizing the metabolic activity of widely applied *in vitro* reporter gene cell lines
71 that are incubated in multi-well plates will help to increase the comparability between the assays
72 and is the first step towards a reliable assessment of the potency of chemicals that are metabolized
73 in HTS *in vitro* reporter gene assays. For MCF-7 cells implemented in the antioxidant response
74 element assay AREc32, fluorescence measurements provided evidence of BaP biotransformation
75 capability,[16] indicating that chemical exposure can induce the expression of CYP enzymes in
76 AREc32, which was observed for native MCF-7 cells during chemical exposure.[17, 18] These studies
77 emphasize the necessity to characterize the metabolic activity of reporter gene cells during
78 exposure to chemicals, whereas investigating the basal metabolic capacity of *in vitro* cells might
79 underestimate their metabolic activity under exposure conditions.
80 For quantitative *in vitro-in vivo* extrapolation (QIVIVE) approaches, characterizing the metabolic
81 activity of the applied *in vitro* reporter gene cell line can clearly support the development of models
82 for human exposure predictions from *in vitro* effect data. *In vitro* hepatic clearance assays with
83 HepaRG and other liver cells can predict metabolic activity in human tissue,[19, 20] and have been
84 implemented in QIVIVE frameworks.[21] Clearance models have been developed that calculate
85 clearance efficiencies of chemicals in blood based on the amount of metabolically active
86 components in S9, microsomal proteins, or hepatocytes.[22] For hepatic assays, cellular metabolism

87 was thoroughly investigated and discussed, however, the link to metabolic processes in *in vitro*
88 reporter gene assays is missing. In studies with *in vitro* reporter gene assays, cellular metabolism
89 was mainly neglected, even for cell lines that were originally developed as models for hepatic
90 metabolism of chemicals.[23] This indicates the necessity to investigate the metabolic activity of *in*
91 *vitro* assays if used for human health risk assessment of chemicals and how to foster its
92 implementation in QIVIVE approaches.
93 This study aimed to characterize cellular metabolism in reporter gene assays to investigate its role
94 in the interpretation and extrapolation of *in vitro* effects. Therefore, we analyzed the *CYP1A1*
95 mRNA expression and applied ethoxyresorufin-O-deethylase (EROD) assays as well as integrated
96 fluorescence microscopy and chemical analysis to track concentrations in the cell and exposure
97 medium. The method was applied to measure the cellular metabolism of BaP in the AREc32, ARE-
98 bla (Antioxidant Response Element) and GR-bla (Glucocorticoid Receptor) reporter gene cell lines
99 that were based on human breast cancer cells (MCF-7), hepatocellular carcinoma cells (HepG2),
100 and human embryonic kidney cells (HEK293), respectively. MCF-7 was originally developed for
101 cancer research[24] and has been widely applied as AREc32[25] for skin sensitization testing[26] and
102 environmental monitoring.[27] The GR-bla and ARE-bla reporter gene cell lines were both
103 implemented in the Tox21 battery of cell-based bioassays.[1] We hypothesized that (i) a difference
104 in the metabolic activity of the cell lines can have a significant influence on chemical exposure in
105 the medium and cells, potentially leading to sensitivity differences between cell lines towards
106 biotransformed chemicals; (ii) exposure to BaP increase *CYP1A1* mRNA expression and total P450
107 CYP1 activity which (iii) leads to an exponential decrease in cellular concentrations of BaP and an
108 increase in metabolite concentrations. We discuss differences in the metabolic activity between the
109 evaluated cell lines considering their tissue origin (breast cancer, kidney, liver) and their relevance
110 for the QIVIVE of biodegradable chemicals measured in *in vitro* reporter gene assays.

111 # 2. Materials and Methods

112 **2.1 Chemicals and cell lines**

113 Benzo(a)pyrene (BaP, ≥96%), 3-hydroxybenzo(a)pyrene (3-OH-BaP, ≥99%), and
114 benzo(a)pyrene-7,8-dihydrodiol-9,10-epoxide (BaP-epoxide, ≥99%) were purchased from Sigma
115 Aldrich. 9-Hydroxybenzo(a)pyrene (9-OH-BaP, ≥99%), (±)-*trans*-4,5-Dihydroxy-4,5-
116 dihydrobenzo(a)pyrene (4,5-OH-BaP, ≥99%), (±)-*trans*-7,8-Dihydroxy-7,8-
117 dihydrobenzo(a)pyrene (7,8-OH-BaP, ≥99%), and *trans*-9,10-Dihydroxy-9,10-dihydroxy-9,10-
118 dihydrobenzo(a)pyrene (9,10-OH-BaP, ≥99%) were acquired from the Biochemical Institute for
119 Environmental Carcinogens. 7-ethoxyresorufin and NaOH (≥98.8 %) were purchased from Th.
120 Geyer and resorufin (95%) and dicoumarol from Merck. TRIS buffer was purchased from
121 AppliChem.

122 **2.2 Cell cultivation and assay conditions**

123 ARE-bla, GR-bla and AREc32 cells were cultivated in Dulbecco's Modified Eagle Medium
124 (DMEM GlutaMAX, Thermo Fisher) amended with 10% fetal bovine serum (FBS) in cell culture
125 flasks. Untreated FBS was used for AREc32 cells and dialyzed FBS for GR-bla and ARE-bla cells.
126 Reaching a confluency of 70 – 90%, the cell number was quantified with a cell counter CASY
127 MODEL TT (Roche Innovatis). The cells were washed twice with phosphate buffered saline (PBS,
128 8% NaCl, 0.2% KCl, 1.442% Na_2HPO_4 and 0.25% KH_2PO_4 in H_2O) and resuspended in DMEM
129 GlutaMAX with 2% untreated FBS. This cell suspension was split into two different treatments:
130 (i) 10 mL were split into five cell culture flasks each and (ii) 90 µL were seeded into each well of
131 poly-D-lysine-coated 96-well polystyrene plates with a clear and flat bottom for GR-bla and ARE-
132 bla and AREc32 was seeded into a tissue culture treated 96-well plate (Corning). The cell numbers
133 were previously optimized and adjusted to 1.5×10^6 (ARE-bla), 9×10^5 (AREc32), and 1.3×10^6 (GR-
134 bla) in the cell culture flasks (25 cm^2 for quantitative PCR) to reach a confluency of 70-90 % after
135 48 h and 15,000 (ARE-bla), 11,000 (AREc32), and 11,000 (GR-bla) in the wells, respectively. The
136 culture flasks and well plates were incubated for 24 h at 37 °C and 5% CO_2 for cell attachment
137 before starting the experiments.

138 **2.3 BaP exposure experiments**

139 The cells were exposed to BaP either in 96-well plates for fluorescence measurement (Section 2.4),
140 chemical analysis (Section 2.5), and EROD measurement (Section 2.7), or in cell culture flasks for
141 *CYP1A1* mRNA expression analysis (Section 2.6). The nominal BaP concentration in the exposure
142 medium was 0.25 mg L^{-1}, which ensured quantifiable concentrations in the medium but did not
143 cause cytotoxicity.[16]

144 Complying with protocols to avoid solvent-associated artefacts in multi-well plates,[28, 29] 30 µL of
145 preequilibrated (>1 h) exposure medium containing 1 mg L^{-1} BaP were pipetted to 90 µL cell
146 suspension of each well, resulting in a final methanol content of 0.5%. For each multi-well plate
147 experiment, three plates containing four sampling time points with 24 replicates were prepared.
148 Additionally, 24 unexposed wells with cells and 24 BaP exposed cell-free wells were prepared and
149 extracted after 24 h of incubation. Fluorescence intensities were measured in 6 well replicates per
150 sampling point as described in Section 2.4. Ten sampling points within 24 h after dosing (0 h, 1 h,
151 2 h, 4 h, 6 h, 8 h, 12 h, 16 h, 20 h, 24 h) per experiment were tested and each cell line was tested in
152 two independent experiments. In each well ten replicate images at different positions were
153 captured. Simultaneously to the fluorescence measurements, the 60 µL exposure medium of 20
154 independent wells were pooled and extracted as described in Section 2.5. In additional experiments,
155 the medium was removed from BaP exposed and unexposed cells (0 h) after 2 h, 4 h, 8 h, 16 h, and
156 24 h for EROD measurements as described in Section 2.7.

157 The culture flasks containing 10 mL medium were dosed by pipetting 45 µL of a methanolic stock
158 solution (55.5 mg L^{-1}) to 5 mL medium which were taken out of the flasks and transferred to sterile
159 falcon tubes. The dosed medium was vortexed and transferred back to the flasks marking the start
160 of the BaP exposure. Three independent biological replicates per cell line were tested. The cells
161 were harvested before (0 h) and after 2 h and 24 h of BaP incubation, and PCR was conducted as
162 described in Section 2.5.

163 **2.4 Fluorescence microscopy to measure cell exposure**

164 The cell exposure to BaP was tracked over time by fluorescence microscopy using a Zeiss PALM
165 CombiSystem (Zeiss) that allowed simultaneous acquisition of bright and fluorescence images of
166 2D cells in 96-well plates. The detailed protocol of image acquisition and analysis is described
167 elsewhere.[16] Briefly, fluorescence emissions at 435 nm were measured in a 7.5 µm Z-layer at ten
168 equally distributed positions in the well, thereby avoiding overlapping of images and capturing of

169 well edges. BaP was excited at 384 nm for 20 ms following detection of emission maxima at
170 different excitation wavelengths. Images were processed in the KNIME workflow from Fischer et
171 al.[16] integrating ImageJ and morphological image operations to discriminate the extra- and
172 intracellular space in the bright-field images, in which the fluorescence intensity in the medium
173 ($FI_{medium\ mask}$) and in the cells ($FI_{cell\ mask}$) was quantified from the fluorescence images. The mean
174 fluorescence intensity in the cells (FI_{cell}) in each well was calculated by subtracting $FI_{medium\ mask}$ from FI_{cell}
175 $_{mask}$, thereby accounting for the overlapping signals that result from the broad Z-layer of 7.5 μm (eq.
176 1).

177 $$FI_{cell} = FI_{cell\ mask} - FI_{medium\ mask} \quad (1)$$

178 **2.5 Analytical determination of medium concentrations of BaP and BaP-metabolites**

179 Conventional solvent extraction followed by high-performance liquid chromatography (HPLC)
180 was used to measure BaP and metabolite concentrations in the exposure medium over the assay
181 duration of 24 h. For detection of 3-OH-BaP, 4,5-OH-BaP, and 7,8-OH-BaP, a PAH LC column
182 (Phenomenex, 100 x 3.0 mm, 2.6 µm) was equipped and coupled to a fluorescence light detector
183 using a H_2O:acetonitrile solvent gradient over 8.2 min (Table S1). For detection of BaP, 3-OH-
184 BaP, 9-OH-BaP, 9,10-OH-BaP, and BaP-epoxide, a ZORBAX Eclipse Plus C18 column (Agilent,
185 4.6 x 100 mm, 5µm) was equipped using a H_2O:acetonitrile solvent gradient over 16.5 min (Table
186 S2). Calibration standards of BaP and metabolites were prepared at a concentration range of 0.0001
187 – 2 mg L^{-1} in acetonitrile. The solvent extraction was optimized to maximize the recovery of BaP
188 and 3-OH-BaP as described in Section S2. For each time point, 100 µL medium of 18 independent
189 wells of the 96-well plate were pooled and transferred to a 4 mL storage vial (neoLab). 1.8 mL
190 ethyl acetate (HPLC grade, Merck) were added and the suspension was shaken horizontally for 15
191 min at 250 rpm on an orbital shaker (MaxQ6000, Thermo Fisher) and centrifuged at 4000 rpm for
192 5 min for phase separation. 1.2 mL of the supernatant was transferred into a 1.5 mL HPLC vial
193 (Th. Geyer) and evaporated to complete dryness under nitrogen. The residues were dissolved in 50
194 µL acetonitrile and BaP and metabolite concentrations in the extracts were quantified by HPLC
195 (Agilent 1260 system).

196 **2.6 CYP1A1 mRNA expression by quantitative real-time PCR**

197 The expression of *CYP1A1* mRNA in the cell lines was measured by quantitative real-time PCR
198 (qPCR). DNA primers for the *CYP1A1* gene and the housekeeping genes *ACTB* and *EEF1A1* were
199 designed using the open source software Primer3 and purchased from Eurofins Genomics (Section
200 S3). The cells were collected as wet pellets with cell numbers varying between 7×10^5 and 6×10^6.
201 RNA isolation from the cells was performed according to standard protocols using the QIAgen
202 RNeasy mini kit and RNA concentrations and purity in the aqueous solution was measured by
203 spectral photometry (Nanodrop, PEQlab Biotechnologies). Prior cDNA synthesis, a DNAse digest
204 of the RNA was performed (Thermo Fisher). For cDNA synthesis 2 µL random hexamer primer
205 were added to 0.35 µg RNA and mixed, centrifuged and incubated for 5 min at 65 °C and
206 immediately chilled on ice. A mixture of 4 µL reaction buffer, 0.5 µL ribonuclease inhibitor, 2 µL
207 dNTPs, and 1 µL RevertAid H Minus reverse transcriptase (Thermo Fisher) was added and the
208 cDNA was synthesized in a thermocycler at 25 °C for 10 min and 42 °C for 75 min. The reaction
209 was stopped at 70 °C for 10 min and the cDNA solution was stored on ice. A qualitative, standard
210 PCR was used beforehand to investigate if the evaluated cell lines express *CYP1A1* mRNA (Section
211 S4).

212 The qPCR reaction was conducted in 96-well fast optical reaction plates (Thermo Fisher) in a
213 StepOne qPCR System (Applied Biosystems) using the SYBR green master mix for detection,
214 containing 1 µL of cDNA mixed with 6.25 µL SYBR green fluorescence solution (Bioline), 4.25
215 µL bidistilled water, and 0.5 µL of forward and reverse primer. The PCR reaction was initiated at
216 95 °C for 10 minutes followed by 40 cycles of 95 °C for 15 s (DNA denaturation), 56 °C for 15 s
217 (annealing) and at 72 °C for 20 s (elongation). Efficiencies of primers were 109.88 % for *CYP1A1*,
218 99.07 % for *ACTB* and 100.80 % for *EEF1A1*. The Primer sequences are reported in Section S3.

219 *CYP1A1* mRNA expression was calculated relative to the reference genes *ACTB* and *EEF1A1* as
220 well as to control cells using the $2^{-\Delta\Delta Ct}$-method.[30, 31] The threshold cycle value (C_q) of the target
221 gene ($C_{q,CYP1A1}$) was subtracted from the C_q of the reference gene ($C_{q,RG}$) to receive $\Delta C_{q,CYP1A1}$ for
222 all samples and cell lines (eq. 2).

223 $$\Delta C_{q,CYP1A1} = C_{q,CYP1A1} - C_{q,RG} \quad (2)$$

224 The $\Delta C_{q,CYP1A1}$ of the BaP exposed cells ($\Delta C_{q,CYP1A1}$ (BaP)) was compared to the control cells
225 ($\Delta C_{q,CYP1A1}$ (control)) (eq. 3) to calculate the fold induction of *CYP1A1* (Ind_{CYP1A1} (0h→24h))
226 during BaP exposure (eq. 4).

227 $$\Delta\Delta C_{q,CYP1A1} = \Delta C_{q,CYP1A1}\ (\mathrm{BaP}) - \Delta C_{q,CYP1A1}\ (\mathrm{control}) \quad (3)$$

228 $$\mathrm{Ind}_{CYP1A1}\ (0\mathrm{h}\rightarrow 24\mathrm{h}) = 2^{-\Delta\Delta C_{q,CYP1A1}} \quad (4)$$

229 **2.7 EROD assay to determine CYP1 enzyme activity**

230 The activity of the CYP1 subfamily enzymes after BaP exposure was measured using the
231 ethoxyresorufin-O-deethylase (EROD) assay that is based on the CYP1-mediated degradation of
232 the 7-ethoxyresorufin (ETX) substrate into the fluorescent resorufin. Further degradation of
233 resorufin was avoided using the reductase inhibitor dicoumarol. A 800 µM ETX stock solution in
234 methanol and a 1 mM dicoumarol stock solution in tris(hydroxymethyl)aminomethane (TRIS)
235 buffer (AppliChem) were used to prepare an ETX working solution of 8 µM ETX + 10 µM
236 dicoumarol in PBS.[32] At each sampling point, the medium was removed from the wells and the
237 wells were rinsed twice with 120 µL PBS. 120 µL of ETX working solution was added to each
238 well. Fluorescence intensity of resorufin (586 nm) was measured after excitation at 571 nm in a
239 preheated microplate reader (plate reader Infinite 200 PRO, Tecan) at 37 °C for 10 min with
240 measurement intervals of 30 s. Cells without BaP exposure and the ETX solution without cells
241 served as negative controls. Liver S9 (0.002 $mg_{protein}\ mL^{-1}$) was applied as positive control. The
242 background fluorescence signal of the ETX negative control was subtracted from the sample wells.
243 The amount of resorufin ($n_{resorufin}$) in the samples were quantified using a linear resorufin calibration
244 curve that was measured in PBS in parallel.[33] The increase of resorufin over the 10-min
245 measurement ($n_{resorufin}\ min^{-1}$) was normalized to the cell number in the well,[34] which was estimated
246 from the increase in the cell mask measured by bright-field imaging using the fluorescence
247 microscope.[16] The measured CYP1 enzyme activities A_{BaP} ($n_{resorufin}\ 10^6\ cells^{-1}$) were plotted against
248 BaP exposure time to fit the slope of the CYP1 enzyme activity rate m_{CYP} ($n_{resorufin}\ h^{-1}\ 10^6\ cells^{-1}$)
249 with linear regression with the y-intercept set to the basal CYP1 enzyme activity measured for the
250 control cells at time 0 ($A_{control,t0}$) (eq. 5).

251 $$A_{\mathrm{BaP}}\ (t) = \mathrm{m}_{\mathrm{CYP}} \cdot t + A_{\mathrm{control}}\ (t0) \quad (5)$$

252 **2.8 Kinetic model to describe chemical transport and metabolism**

253 We hypothesized that the chemical fate of BaP in the assay system depends on (i) the chemical
254 partitioning between the medium and the cells and (ii) the elimination of the chemical in the cells
255 (Figure 1). Volatilization of BaP could be neglected because the medium-air partition constant

256 $K_{medium/air}$ of BaP is more than four orders of magnitude higher than the threshold where evaporative
257 losses would be expected (log $K_{medium/air}$ of 10^4).[35] Furthermore, in 96-well plates and medium
258 supplemented with 2% medium the loss to the polystyrene of the well-plate is expected to be
259 <2%.[36] A two-compartment model was applied to characterize the metabolic activity of the cells
260 that integrates these two kinetic processes and sequentially fits first-order uptake ($k_{medium\rightarrow cell}$, h^{-1})
261 and elimination ($k_{cell\rightarrow medium}$, h^{-1}) rate constants of the parent in non-metabolically active cells.
262 These rate constants were then fixed to derive the metabolic rate constant k_{met} (h^{-1}) from the
263 experimental FI_{cell} over time. The FI_{cell} was assumed to be the sum of the fluorescence signal of
264 BaP and its fluorescent metabolites and its decrease expressed as k_{met} can be related to the formation
265 of non-fluorescent metabolites. The metabolites are also eliminated from the cell, but this process
266 could not be detected with the fluorescence method applied in this study. Preliminary emission
267 measurements showed that BaP and all evaluated metabolites show fluorescence emission at 435
268 nm, which was the emission wavelength captured by the fluorescence microscope (Section S5).
269 The emission scans of the monohydroxylated BaP metabolites and BaP showed considerably
270 higher fluorescence emission than the dihydroxylated metabolites and the BaP-epoxide (Figure
271 S4). For instance, the BaP fluorescence was ~18x higher than the fluorescence of the BaP-epoxide.
272 Following the results of the emission scans, the decrease in FI_{cell} and FI_{medium} in our experiments
273 was ascribed to the metabolization of BaP and the primary metabolites (monohydroxylated BaPs)
274 to the secondary metabolites 4,5- , 7,8- and 9,10-dihydroxy-BaP and the BaP-epoxide (Figure 1).

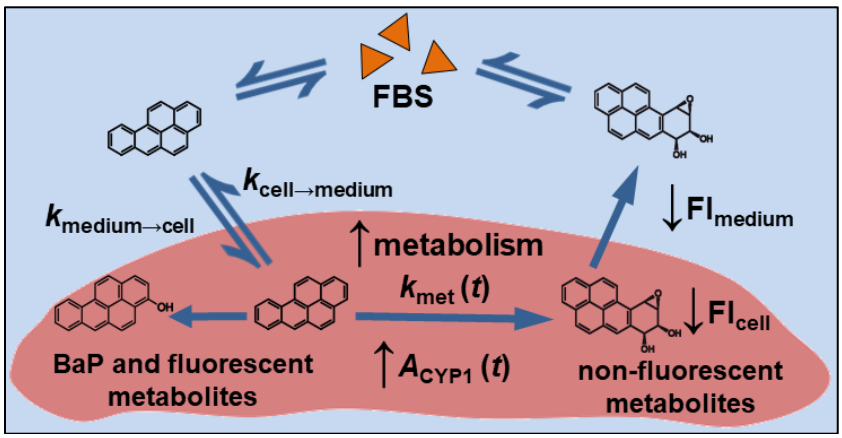

275
276 **Figure 1** Kinetic processes between and within the exposure medium (blue) and the cells (red) in
277 *in vitro* reporter gene assays. The parent chemical in the medium is taken up by the cells
278 ($k_{medium\rightarrow cell}$), metabolized ($k_{met}$) based on the availability and induction of CYP1 enzymes and both,
279 the BaP and its metabolites, are released into the medium ($k_{cell\rightarrow medium}$). The FBS in the medium
280 binds the parent chemical and excreted metabolites.

281 As medium and cells are in permanent contact, changes in FI_{medium} and FI_{cell} over time t can be
282 described by two coupled differential equations (eqs. 6 and 7).

283 $$\frac{dFI_{medium}}{dt} = k_{cell\rightarrow medium} \cdot FI_{cell}(t) - k_{medium\rightarrow cell} \cdot FI_{medium}(t) \quad (6)$$

284 $$\frac{dFI_{cell}}{dt} = k_{medium\rightarrow cell} \cdot FI_{medium}(t) - (k_{cell\rightarrow medium} + k_{met}\ (t)) \cdot FI_{cell}(t) \quad (7)$$

285 $k_{medium\rightarrow cell}$ and $k_{medium\rightarrow cell}$ are the first-order rate constants (h^{-1}) that describe the kinetics of
286 chemical partitioning of the sum of the fluorescent species between the medium and cells. For cells
287 that are not metabolic active, $k_{cell\rightarrow medium}$ and $k_{medium\rightarrow cell}$ can be fitted from FI_{medium} (t) and FI_{cell} (t)
288 by setting $k_{met} = 0$. We accounted for a temporal increase in the basal k_{met} because it is dependent
289 on the increase in CYP1 activity (m_{CYP}) compared to unexposed cells ($A_{control}$) assuming a linear
290 relationship between enzyme activity rate constant $\frac{m_{CYP}}{A_{control}}$ and time (eq. 8).

291 $$k_{met}\ (t) = k_{met} \cdot t \cdot \frac{m_{CYP}}{A_{control}} \quad (8)$$

292 The experimental FI_{medium} and FI_{cell} of AREc32, ARE-bla, and GR-bla cells were fitted with eqs. 6
293 and 7 using the damped least-squares (DLS) method for multiparameter fitting, yielding the
294 derivation of $k_{medium\rightarrow cell}$, $k_{medium\rightarrow cell}$, and k_{met}. As the fit robustness decreased substantially with
295 each added fit variable, we first fitted $k_{medium\rightarrow cell}$ and $k_{medium\rightarrow cell}$ using the FI_{medium} and FI_{cell} of the
296 metabolic inactive GR-bla cells, and resulting $k_{medium\rightarrow cell}$, $k_{medium\rightarrow cell}$ were subsequently applied to
297 fit k_{met} of the metabolic active AREc32 and ARE-bla cells. The fit program was set up in R Studio
298 Version 1.2.5019 and is reported in the Supporting Information, Section S6.

299 # 3. Results and Discussion

300 **3.1 Basal and exposure-induced expression of *CYP1A1* and activity of CYP1 enzymes**

301 *CYP1A1* mRNA were identified with standard PCR analysis in all three evaluated reporter gene
302 cell lines in absence of BaP, (Section S4) agreeing with *CYP* studies on native MCF-7, HepG2,
303 and HEK293 cells.[12, 13] As *CYP1A1* is described as the dominant and most abundant target enzyme
304 of the AhR receptor and the metabolism of aromatic hydrocarbons like BaP[37] and considering that
305 *CYP1A1* is involved in ~75% of the biodegradation processes of xenobiotics,[7, 8] we focused on
306 *CYP1A1* gene expression as indicator gene for cellular metabolism. The qPCR analysis indicated
307 that the basal expression of *CYP1A1* mRNA, reported as $\Delta C_{q,CYP1A1}$, was relatively stable over time
308 from 0 to 24 h in all cell lines in chemical-free exposure medium (Figure S5 in Section S7). The
309 basal expression of *CYP1A1* without BaP exposure was 300 and 1000 times higher in ARE-bla
310 compared to the AREc32 and GR-bla cells after 24 h (Figure 2A). Consistently, the basal EROD
311 activity in absence of BaP was ~26× and ~5× higher in ARE-bla and AREc32 than in GR-bla,
312 respectively. Note that the $\Delta C_{q,CYP1A1}$ and corresponding Ind_{CYP1A1} values (Figure 2A) are not entirely
313 comparable due to variabilities in the expression of the control gene between the cell lines,[31, 38] but
314 there remain substantial differences between the high Ind_{CYP1A1} of 1,220 for AREc32 and the low
315 Ind_{CYP1A1} of 11 for ARE-bla, that cannot be caused by this experimental variability.

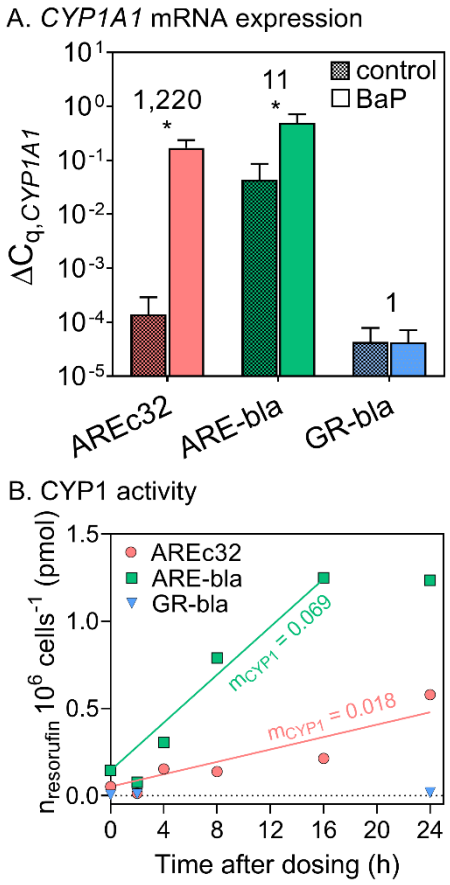

Figure 2A. Expression of *CYP1A1* mRNA ($\Delta C_{q,CYP1A1}$, bars) and Ind_{CYP1A1} (reported numbers over bars) in AREc32, ARE-bla, and GR-bla after 24 h of incubation in chemical-free (control, dotted bars) or BaP spiked medium (clear bars) with significant differences between the treatments marked with an asterisk ($p < 0.05$, unpaired t-test in GraphPad PRISM, v. 8.3). **B.** Basal and BaP-induced CYP1 activity over 24 h BaP exposure and corresponding fit (r^2 (AREc32) = 0.83; r^2 (ARE-bla) = 0.94) that was used in the kinetic model to describe the increase in CYP1 activity m_{CYP1} (eq. 8), with experimental basal activities $A_{control}$ of 0.003±0.005 (GR-bla), 0.051±0.023 (AREc32), and 0.143±0.051 (ARE-BLA) (n = 5). For ARE-bla, the 24 h measurement point was not included in the linear fit.

The qPCR showed that BaP exposure significantly induced *CYP1A1* expression in AREc32 ($p = 0.01$) and ARE-bla ($p = 0.02$) cells but not in GR-bla cells ($p = 0.99$, Figure 2A, unpaired t-test), which also lead to an increase in the EROD activity over the 24 h assay (Figure 2B). The resulting *CYP1A1* expression was similar for AREc32 and ARE-bla but since basal levels differed, the *CYP1A1* expression induced by BaP led to an Ind_{CYP1A1} of 71 after 2 h and 1,220 after 24 h of BaP exposure in AREc32 but only a 11× increase in ARE-bla after 24 h (Figures 2A and S6). For ARE-bla levels of *CYP1A1* gene expression were higher after 2 h (Ind_{CYP1A1} = 26) than at 24 h exposure (Ind_{CYP1A1} = 11, Figure S5A). This difference between the cell lines was expected, as HepG2

334 (ARE-bla) and MCF-7 (AREc32) cells were reported to be highly sensitive to *CYP* gene induction
335 by chemicals,[12, 14] whereas kidney cells (HEK293 for GR-bla) were not expressing *CYP1A1* to a
336 measurable extent.[13]
337 Consistent with induced *CYP1A1* expression, the EROD activity increased linearly in AREc32
338 whereas it remained constant for GR-bla during BaP exposure (Figure 2B). The increased basal
339 and chemical-induced expression and activity of CYP1 enzymes in the cancer cell lines AREc32
340 and ARE-bla could also be the result of p53-BaP complex binding as p53 transcription factors are
341 upregulated in tumor cells compared to normal tissue.[39] While *CYP1A1* expression did not increase
342 in GR-bla during BaP exposure, it can be noted that GR-bla have a basal *CYP1A1* gene expression
343 and a basal CYP1 activity, which appears not be influenced by BaP exposure (Figure S5C). As
344 AhR receptors were identified in kidney tissue, the signaling pathway of the ligand-AhR complex
345 and following binding to the XRE transcription factor might be interrupted in GR-bla cells.[40] The
346 analysis of BaP-induced *CYP1A1* mRNA expression and CYP1 EROD activity demonstrated that
347 (i) the basal metabolic capacity of the reporter gene cell lines can substantially differ and (ii) that
348 the metabolic activity of reporter gene cell lines can vary greatly over the typical assay duration in
349 presence of AhR ligands.

350 **3.2 Temporal BaP and metabolite concentrations in the exposure medium**

351 BaP concentrations in the exposure medium ($C_{medium,BaP}$) of ARE-bla and AREc32 decreased
352 considerably over the 24-h experiments whereas it remained constant in the GR-bla assay (Figure
353 3A). This observation agreed well with the high basal and BaP-induced expression of *CYP1A1* and
354 CYP1 EROD activity in ARE-bla and AREc32 and the low *CYP1A1* expression in GR-bla (Figure
355 2A). Even though the decrease in $C_{medium,BaP}$ was similar in AREc32 and ARE-bla over the first 8 hours,
356 the decrease in $C_{medium,BaP}$ is more pronounced in ARE-bla after 12 h compared to AREc32. Still, BaP
357 decreased linearly in both cell lines. The linear decrease of $C_{medium,BaP}$ in AREc32 matches the *CYP1A1*
358 mRNA expression levels (Figure 2A) and the linearly increasing CYP1 activity (Figure 2B). For
359 ARE-bla, the basal expression of *CYP1A1* was almost as high as for AREc32 after 24 h and the
360 increase of the CYP1 activity (m_{CYP1}) was >2× higher, which explains the faster decrease in $C_{medium,BaP}$
361 in ARE-bla.

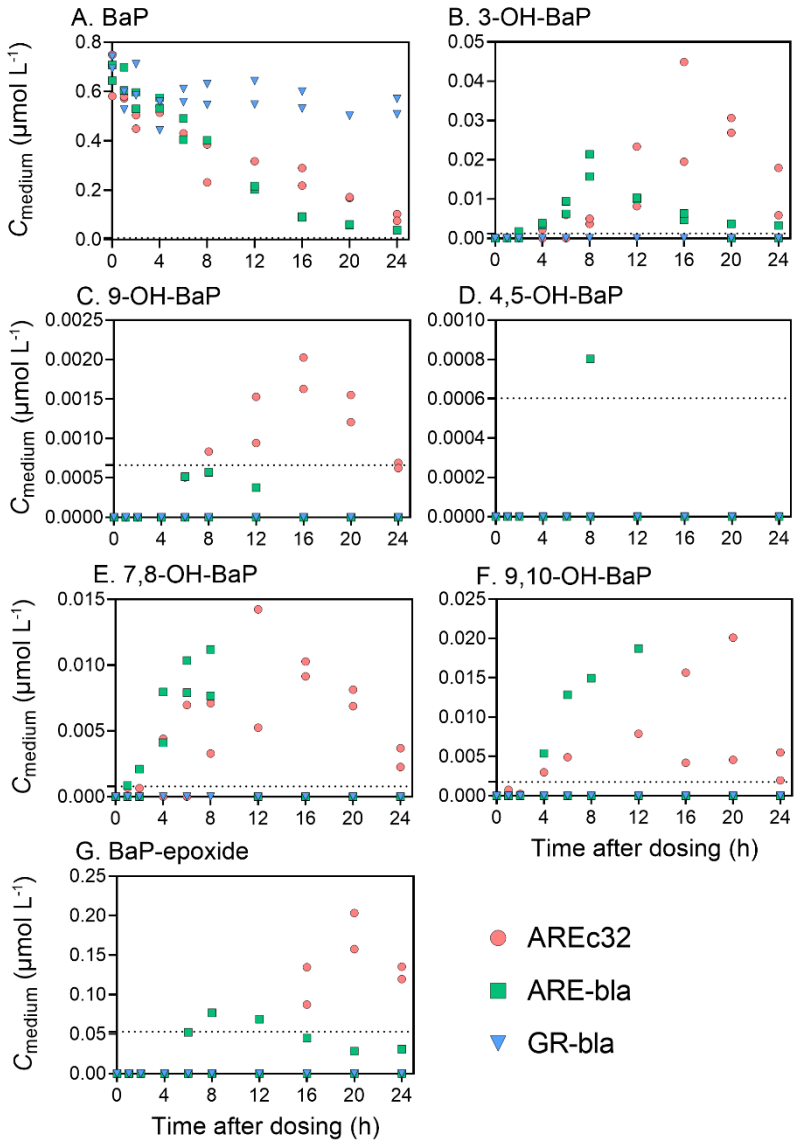

362

363 **Figure 3** BaP and metabolite concentrations measured over time in the exposure medium (C_{medium})
364 of AREc32, ARE-bla, and GR-bla cells. The dotted lines indicate the limits of detection (LOD)
365 for each chemical in the HPLC measurements.

366 Given that the BaP metabolites were not detected in GR-bla cells that were tested with the same
367 experimental setup, the continuous reduction in $C_{medium,BaP}$ in AREc32 and ARE-bla stemmed from
368 cellular metabolism and was evidenced by substantial metabolite formation (Figures 3B-G). Stable
369 mono- and dihydroxylated BaP served as indicators for *in vitro* metabolism of BaP. Although it is
370 more challenging to quantify BaP metabolites with limited stability as the BaP-epoxide,[41] we were
371 able to quantify the BaP-epoxide in concentrations of 0.05-0.2 μmol L^{-1} in the medium of AREc32
372 and ARE-bla. The BaP-epoxide was first detected after 6 h in ARE-bla and after 16 h in AREc32,

373 respectively, indicating that the transformation of BaP in AREc32 is slower compared to ARE-bla
374 (Figure 3G), further evidenced by the earlier detection of mono- and dihydroxylated BaP
375 metabolites in ARE-bla than in AREc32 (Figures 3B-F). After 12 h, these metabolites were no
376 longer detected in ARE-bla and C_{medium} of the BaP-epoxide was likewise decreasing, agreeing with
377 the observation that the CYP activity of ARE-bla remains stable between 16 and 24 h (Figure 2B).
378 Interestingly, the C_{medium} of 7,8-OH-BaP increased substantially in the first 8 h in ARE-bla but was
379 not detected after 12 h (Figure 3E), at which C_{medium} of the BaP-epoxide was detected (Figure 3G).
380 Likewise, 7,8-OH-BaP concentrations decreased with increasing BaP-epoxide concentrations in
381 AREc32 after 12 h. 7,8-OH-BaP was shown to be transformed into the BaP-epoxide in rat liver
382 microsomes[42] and our results indicate that this metabolic pathway is likewise present in human *in*
383 *vitro* cells. The molar mass balance of BaP and metabolites ascribed ~15% of the reduction in
384 $C_{medium,BaP}$ to the transformation to the BaP-epoxide in ARE-bla after 12 h and ~20% for AREc32 after
385 24 h. The formation of 3-OH-BaP, 9-OH-BaP, 4,5-OH-BaP, and 9,10-OH-BaP contributed < 2%
386 to the mass balance, but the continuous decrease in C_{medium} of BaP and all evaluated metabolites
387 indicates further degradation of the transformation products. *In vivo*, glucuronyl conjugates are
388 formed that are excreted in urine.[43] Our results indicate that BaP is metabolized in AREc32 and
389 ARE-bla to various intermediate and end products, still, a comprehensive investigation of the
390 metabolic pathway would require the measurement of additional metabolites, which was outside
391 the scope of this study.

392 **3.3 Fluorescence kinetics in cells and exposure medium**

393 Measuring the emission wavelengths of BaP and all evaluated chemicals revealed that the BaP and
394 monohydroxylated BaP metabolites exhibited a substantially higher fluorescence intensity than
395 the dihydroxylated metabolites and the BaP-epoxide at the wavelength captured by the
396 fluorescence microscope (435 nm) (Figure S4). Therefore, we interpreted FI_{cell} and FI_{medium} as a
397 proxy of the total concentration of BaP and monohydroxylated BaP metabolites, while ascribing a
398 decrease in FI_{medium} and FI_{cell} to a further metabolization to dihydroxylated BaP and the BaP-
399 epoxide or similar structures.

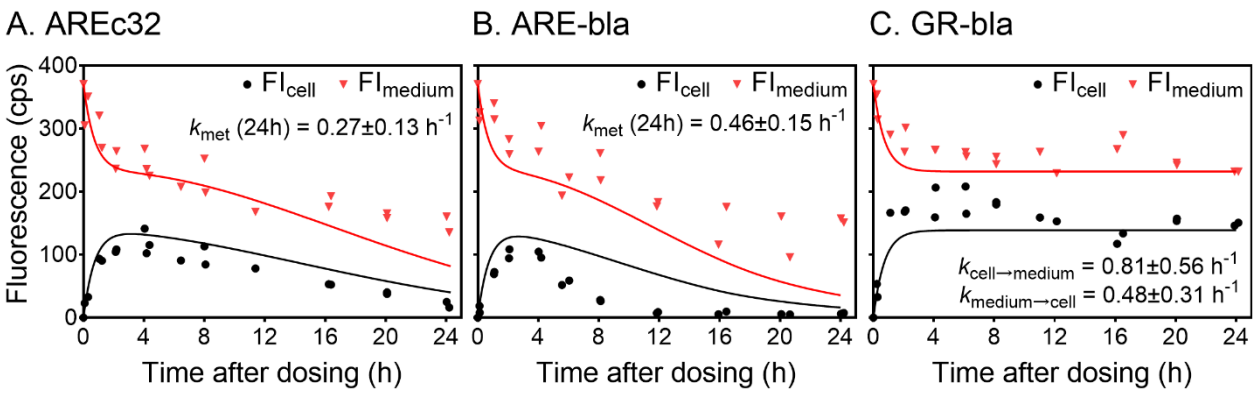

Figure 4 Fluorescence intensities (FI_{cell}, black dots) in AREc32 (A.), ARE-bla (B.), and GR-bla (C.) cells and corresponding fluorescence intensities in the exposure medium (FI_{medium}, red triangles) over 24 h. FI_{cell} and FI_{medium} were fitted with eqs. 6 and 7 to derive medium-cell partitioning and metabolic rates for the cells.

Uptake of BaP by *in vitro* cells was reported to take ~2 h to reach equilibrium with 2% FBS in the exposure medium.[16] We were able to reproduce these findings for the evaluated cell lines that all reached a maximum FI_{cell} within 2 h (Figure 4). The maximum of FI_{cell} in GR-bla cells remained constant until the end of the experiment (24 h). Contrarily, FI_{cell} in AREc32 and ARE-bla continuously decreased after reaching the maximum after ~2 h. Considering the constant medium and incubation conditions applied for all three evaluated cell lines as well as the high basal and exposure-induced expression of *CYP1A1* encoding mRNA and EROD activity in AREc32 and ARE-bla (Figure 2), we can attribute this decrease in cell exposure to cellular metabolism. The maximum FI_{cell} was lower for AREc32 and ARE-bla than for GR-bla. Since the steady-state without metabolism should be independent of the cell line, we can assume that the reduction of the maximum FI_{cell} was caused by metabolism.

The experimental FI_{cell} and FI_{medium} of the cell lines were fitted using eqs. 6 and 7 as described in Section 2.8. The resulting k_{met} and corresponding fits describe the experimental FI_{cell} and FI_{medium} reasonably well (SE reported in Figure 4). A possible error in the model is that FI_{cell} and FI_{medium} are mixed signals of BaP and foremost monohydroxylated metabolites (Figure S4). For fitting of k_{met}, we used the $k_{medium\rightarrow cell}$ and $k_{medium\rightarrow cell}$ determined for the metabolic inactive GR-bla cells (eq. 7). These k might not represent the chemical partitioning of BaP metabolites between medium and cells, which would explain why the fit deviates from the experimental FI_{cell} and FI_{medium} to a higher extent towards the end of the experiment, at which a higher proportion of the measured fluorescence signal is expected to result from BaP metabolites (Figures 3B-G).

425 The transport and metabolism of chemicals in *in vitro* reporter gene assays is influenced by several
426 factors (Figure 1). As shown in earlier studies, the medium is the dominant sorptive reservoir in
427 the assays that can continuously deliver chemicals into the cells.[44] After dosing of the chemicals
428 into the medium, they can be taken up by the cells by passive diffusion through the membranes
429 and potentially by active co-transport by FBS endocytosis,[16] visible in our experiments in the
430 increasing FI_{cell} over the first 2 h after chemical dosing (Figure 4). The maximum FI_{cell} in GR-bla
431 was attained faster (after ~1 h) and was considerably higher than the maximum FI_{cell} in ARE-bla
432 and AREc32 (~160 cps compared to ~104 cps after ~2 h). In these metabolic active cells, the
433 kinetics of metabolism are concurrent with the uptake kinetics of BaP from the medium, leading
434 to the observed turning point after ~4 h at which BaP degradation is faster or cancels out BaP
435 uptake (Figures 4A and B). The BaP exposure led to an increase in *CYP1A1* expression in AREc32
436 and ARE-bla (Figure 2), increasing the metabolic rate and exponentially decreasing FI_{cell} over time,
437 which was observed for ARE-bla (Figure 4B) but not for AREc32 cells in our experiments (Figure
438 4A). The measured amount of *CYP1A1* mRNA in AREc32 was a factor of 14 lower than in ARE-
439 bla after 2 h and a factor of 3 lower after 24 h, which would explain that FI_{cell} in ARE-bla decreased
440 to unexposed cell levels after 12 h while FI_{cell} was still measurable after 24 h in AREc32. FI_{cell} and
441 FI_{medium} were constant for GR-bla after chemical equilibrium between the cells and medium was
442 achieved (Figure 4C). This does not necessarily mean that GR-bla cells are completely uncapable
443 of biotransformation, as evidenced by their measurable basal EROD activity (Figure 2B), but their
444 metabolic activity is too low to measure a significant decrease in FI_{cell} and FI_{medium} in our experiments.

445 **3.4 Relevance of *in vitro* metabolism for high-throughput screening**

446 Our experiments demonstrated the complexity and variability of *in vitro* metabolism over time and
447 between reporter gene assays that implement different cell lines. The difference of metabolic
448 activity of *in vitro* reporter gene assays can reduce their significance and comparability, as variable
449 exposure can occur dependent on the metabolic capacity of the cell line applied. In *in vitro* effect
450 databases, effect concentrations are generally reported for each chemical, such as the 50% activity
451 concentrations (AC_{50}) in the Tox21 database. These AC_{50} are based on nominal concentrations, i.e.,
452 those dosed to the system and will be affected by *in vitro* metabolism of the evaluated chemical to
453 different degrees depending on the metabolic activity of the cells during the assay. Furthermore,
454 many chemicals are only biologically active after metabolic activation. Eventually, the cells are

455 exposed to the parent chemical that is redelivered from the medium as well as to its metabolites
456 (Figure 1). The extent and chronology of exposure depends on the metabolic activity of the applied
457 cell line, potentially leading to variable AC_{50} of the same chemicals in different assays that are not
458 resulting from differences in the sensitivity of the receptor but from varying exposure conditions.
459 For instance, the antioxidant response element (ARE) is implemented in MFC-7 cells (AREc32
460 assay) and HepG2 cells (ARE-bla assay), thus effects of chemicals that are metabolized by the
461 cytochrome P450 enzyme complex might be less comparable between the assays, as shown
462 exemplarily for BaP in this study. Accounting for the metabolic activity of *in vitro* reporter gene
463 cells would enhance the interpretability of effect data of the biotransformation of chemicals. As
464 shown for AREc32, it is generally not sufficient to measure the basal metabolic capacity in absence
465 of chemical exposure but measuring the induction of relevant enzymes during exposure to AhR
466 ligands is needed. This study focused on CYP1A1 mRNA expression and CYP1 enzyme activity.
467 More data is needed on the expression and the activity of other CYPs and other enzyme families
468 involved in the metabolism of chemicals to comprehensively characterize the metabolic activity
469 of *in vitro* reporter gene cell lines. Existing effect data could be corrected for the metabolic rate of
470 the evaluated chemical by deriving the area under the curve that accounts for the reduced cell
471 exposure of the parent chemical over time. However, it can be expected that the metabolic activity
472 of the cells is not only dependent on their biological origin, but also on the composition and volume
473 of the medium applied as well as the test vessels used, as differences in the cellular health and
474 growth were observed for 2D cultures at different FBS contents[16] and in different multi-well plate
475 materials.[45] The immortalization of *in vitro* cells can lead to an upregulated expression of CYP
476 enzymes,[46] which agrees with the general observation of a high CYP enzyme activity in cancer
477 cells.[39] An experimental approach targeting the assessment of the parent chemical would be to
478 inhibit the metabolic activity of the cells, e.g., by the chemical piperonyl butoxide,[47] but bears the
479 risk for mixture effects between the metabolism inhibitor and the tested chemical.

480 **3.5 Integration of *in vitro* metabolism in quantitative *in vitro-in vivo* models**

481 In studies targeting the extrapolation of *in vitro* effects (QIVIVE), *in vitro* metabolism is generally
482 desired to mimic the realistic exposure conditions in the human body. Even though metabolism is
483 one of the key parameters to predict blood concentrations *in vivo*,[48-50] *in vitro* metabolism was so far
484 neglected in most QIVIVE studies. A mathematical extrapolation of *in vitro* metabolism to *in vivo*

485 exposure scenarios was recently derived, however, under the premise that *in vitro* and *in vivo* cells
486 are equally metabolic active,[22] so far not accounting for differences in the metabolic activity of 2D
487 and 3D cell cultures. For improved QIVIVE of biodegradable chemicals, we need to achieve
488 comparable (not equal) metabolic activities *in vitro* and *in vivo*. Experimental metabolic clearance
489 rates of well-studied AhR and p53 ligands would enable the derivation of correction factors that
490 account for differences in the metabolic activity of cells *in vitro* and *in vivo*, and could be
491 implemented in existing QIVIVE models.[22] An experimental solution would be to combine reporter
492 gene assays with S9 proteins for which metabolic clearance rates are well-documented,[51] either
493 directly in the exposure medium during incubation, or in a fraction of the medium that is
494 subsequently dose the sample on the cells. The application of S9 proteins would mimic the
495 enzymatic degradation by the liver and could represent exposure conditions suitable for
496 extrapolation to the realistic *in vivo* situation. For *in vitro* assays that apply protein- and lipid-rich
497 FBS in the medium, *in vitro* metabolic clearance always needs to be related to the total medium
498 concentrations and not solely based on the free fraction. The chemicals sorbed to the medium FBS
499 can desorb to the water phase of the medium, effectively being likewise accessible for
500 biotransformation. Furthermore, the co-transport of chemicals by FBS endocytosis can increase
501 the concentration in the cells, which had been already indicated,[16] a scenario that might be
502 comparable to the chemical exposure of *in vivo* cells over human serum albumin in blood.[52]

503 **Corresponding author**

504 * Address: Helmholtz Centre for Environmental Research - UFZ, Department Cell Toxicology,
505 Permoserstraße 15, 04318 Leipzig, Germany; Phone: +49 341 235 – 1244; E-Mail address:
506 beate.escher@ufz.de

507 **Acknowledgements**

508 We thank Satoshi Endo and Joop Hermens for reviewing the manuscript and Mirco Bundschuh for
509 useful comments on the study. The laboratory support from Peggy Wellner and Nicole Schweiger
510 are greatly appreciated. We thank the Centre for Chemical Microscopy (ProVIS) at the Helmholtz
511 Centre for Environmental Research supported by European Regional Development Funds (EFRE–

512 Europe funds Saxony) for providing their analytical facilities. We gratefully acknowledge the
513 financial support of the CEFIC Long-Range Research Initiative (LRI), project ECO36.

514 **References**

515 (1) Attene-Ramos, M. S., Miller, N., Huang, R., Michael, S., Itkin, M., Kavlock, R. J., Austin, C. P., Shinn, P.,
516 Simeonov, A., Tice, R. R., and Xia, M. (2013) The Tox21 robotic platform for the assessment of
517 environmental chemicals - from vision to reality. *Drug Discovery Today 18*, 716-723.

518 (2) Huang, R., Xia, M., Cho, M.-H., Sakamuru, S., Shinn, P., Houck, K. A., Dix, D. J., Judson, R. S., Witt, K.
519 L., and Kavlock, R. J. (2011) Chemical genomics profiling of environmental chemical modulation of human
520 nuclear receptors. *Environmental health perspectives 119*, 1142-1148.

521 (3) Kim, J. H., Stansbury, K. H., Walker, N. J., Trush, M. A., Strickland, P. T., and Sutter, T. R. (1998)
522 Metabolism of benzo [a] pyrene and benzo [a] pyrene-7, 8-diol by human cytochrome P450 1B1.
523 *Carcinogenesis 19*, 1847-1853.

524 (4) Miller, K. P., and Ramos, K. S. (2001) Impact of cellular metabolism on the biological effects of benzo [a]
525 pyrene and related hydrocarbons. *Drug metabolism reviews 33*, 1-35.

526 (5) Charles, G. D., Bartels, M. J., Zacharewski, T. R., Gollapudi, B. B., Freshour, N. L., and Carney, E. W.
527 (2000) Activity of Benzo[a]pyrene and Its Hydroxylated Metabolites in an Estrogen Receptor-α Reporter
528 Gene Assay. *Toxicol Sci 55*, 320-326.

529 (6) Frizzell, C., Uhlig, S., Miles, C. O., Verhaegen, S., Elliott, C. T., Eriksen, G. S., Sørlie, M., Ropstad, E., and
530 Connolly, L. (2015) Biotransformation of zearalenone and zearalenols to their major glucuronide metabolites
531 reduces estrogenic activity. *Toxicol in Vitro 29*, 575-581.

532 (7) Guengerich, F. P. (2008) Cytochrome P450 and chemical toxicology. *Chemical Research in Toxicology 21*,
533 70-83.

534 (8) Meunier, B., de Visser, S. P., and Shaik, S. (2004) Mechanism of oxidation reactions catalyzed by
535 cytochrome P450 enzymes. *Chemical reviews 104*, 3947-3980.

536 (9) Lin, J. H. (2006) CYP induction-mediated drug interactions: in vitro assessment and clinical implications.
537 *Pharmaceutical research 23*, 1089-1116.

538 (10) Hines, R. N., Mathis, J. M., and Jacob, C. S. (1988) Identification of multiple regulatory elements on the
539 human cytochrome P450IA1 gene. *Carcinogenesis 9*, 1599-1605.

540 (11) Iwanari, M., Nakajima, M., Kizu, R., Hayakawa, K., and Yokoi, T. (2002) Induction of CYP1A1, CYP1A2,
541 and CYP1B1 mRNAs by nitropolycyclic aromatic hydrocarbons in various human tissue-derived cells:
542 chemical-, cytochrome P450 isoform-, and cell-specific differences. *Arch Toxicol 76*, 287-298.

543 (12) Jørgensen, E. C. B., and Autrup, H. (1995) Effect of a negative regulatory element (NRE) on the human
544 CYP1A1 gene expression in breast carcinoma MCF-7 and hepatoma HepG2 cells. *Febs Lett 365*, 101-107.

545 (13) Knights, K. M., Rowland, A., and Miners, J. O. (2013) Renal drug metabolism in humans: the potential for
546 drug-endobiotic interactions involving cytochrome P450 (CYP) and UDP-glucuronosyltransferase (UGT).
547 *Br J Clin Pharmacol 76*, 587-602.

548 (14) Choi, J. M., Oh, S. J., Lee, S. Y., Im, J. H., Oh, J. M., Ryu, C. S., Kwak, H. C., Lee, J.-Y., Kang, K. W., and
549 Kim, S. K. (2015) HepG2 cells as an in vitro model for evaluation of cytochrome P450 induction by
550 xenobiotics. *Archives of Pharmacal Research 38*, 691-704.

551 (15) Shah, U. K., Seager, A. L., Fowler, P., Doak, S. H., Johnson, G. E., Scott, S. J., Scott, A. D., and Jenkins, G.
552 J. (2016) A comparison of the genotoxicity of benzo[a]pyrene in four cell lines with differing metabolic
553 capacity. *Mutat Res Genet Toxicol Environ Mutagen 808*, 8-19.

554 (16) Fischer, F. C., Abele, C., Droge, S. T. J., Henneberger, L., König, M., Schlichting, R., Scholz, S., and Escher,
555 B. I. (2018) Cellular uptake kinetics of neutral and charged chemicals in in vitro assays measured by
556 fluorescence microscopy. *Chemical Research in Toxicology*.

557 (17) Ptak, A., Ludewig, G., Rak, A., Nadolna, W., Bochenek, M., and Gregoraszczuk, E. L. (2010) Induction of
558 cytochrome P450 1A1 in MCF-7 human breast cancer cells by 4-chlorobiphenyl (PCB3) and the effects of
559 its hydroxylated metabolites on cellular apoptosis. *Environ Int 36*, 935-941.

560 (18) Spink, B. C., Hussain, M. M., Katz, B. H., Eisele, L., and Spink, D. C. (2003) Transient induction of
561 cytochromes P450 1A1 and 1B1 in MCF-7 human breast cancer cells by indirubin. *Biochem Pharmacol 66*,
562 2313-2321.

563 (19) Guillouzo, A., Corlu, A., Aninat, C., Glaise, D., Morel, F., and Guguen-Guillouzo, C. (2007) The human
564 hepatoma HepaRG cells: a highly differentiated model for studies of liver metabolism and toxicity of
565 xenobiotics. *Chemico-biological interactions 168*, 66-73.

566 (20) Iwatsubo, T., Hirota, N., Ooie, T., Suzuki, H., Shimada, N., Chiba, K., Ishizaki, T., Green, C. E., Tyson, C.
567 A., and Sugiyama, Y. (1997) Prediction of in vivo drug metabolism in the human liver from in vitro
568 metabolism data. *Pharmacology & therapeutics 73*, 147-171.

569 (21) Wetmore, B. A., Wambaugh, J. F., Ferguson, S. S., Li, L., Clewell III, H. J., Judson, R. S., Freeman, K., Bao,
570 W., Sochaski, M. A., and Chu, T.-M. (2013) Relative impact of incorporating pharmacokinetics on predicting
571 in vivo hazard and mode of action from high-throughput in vitro toxicity assays. *Toxicol Sci 132*, 327-346.

572 (22) Krause, S., and Goss, K.-U. (2018) In Vitro–in Vivo Extrapolation of Hepatic Metabolism for Different
573 Scenarios-a Toolbox. *Chemical research in toxicology 31*, 1195-1202.

574 (23) Comenges, J. Z., Joossens, E., Benito, J. S., Worth, A., and Paini, A. (2017) Theoretical and mathematical
575 foundation of the virtual cell based assay–a review. *Toxicol in Vitro 45*, 209-221.

576 (24) Wolf, D. M., and Jordan, V. C. (1994) The estrogen receptor from a tamoxifen stimulated MCF-7 tumor
577 variant contains a point mutation in the ligand binding domain. *Breast Cancer Research and Treatment 31*,
578 129-138.

579 (25) Wang, X. J., Hayes, J. D., and Wolf, C. R. (2006) Generation of a stable antioxidant response element-driven
580 reporter gene cell line and its use to show redox-dependent activation of nrf2 by cancer chemotherapeutic
581 agents. *Cancer Res 66*, 10983-10994.

582 (26) Natsch, A., and Emter, R. (2007) Skin Sensitizers Induce Antioxidant Response Element Dependent Genes:
583 Application to the In Vitro Testing of the Sensitization Potential of Chemicals. *Toxicol Sci 102*, 110-119.

584 (27) Escher, B. I., Dutt, M., Maylin, E., Tang, J. Y. M., Toze, S., Wolf, C. R., and Lang, M. (2012) Water quality
585 assessment using the AREc32 reporter gene assay indicative of the oxidative stress response pathway. *J*
586 *Environ Monitor 14*, 2877-2885.

587 (28) Fischer, F. C., Henneberger, L., Schlichting, R., and Escher, B. I. (2019) How To Improve the Dosing of
588 Chemicals in High-Throughput in Vitro Mammalian Cell Assays. *Chemical Research in Toxicology 32*,
589 1462-1468.

590 (29) Tanneberger, K., Rico-Rico, A., Kramer, N. I., Busser, F. J. M., Hermens, J. L. M., and Schirmer, K. (2010)
591 Effects of Solvents and Dosing Procedure on Chemical Toxicity in Cell-Based in Vitro Assays.
592 *Environmental Science & Technology 44*, 4775-4781.

593 (30) Livak, K. J., and Schmittgen, T. D. (2001) Analysis of Relative Gene Expression Data Using Real-Time
594 Quantitative PCR and the 2−ΔΔCT Method. *Methods 25*, 402-408.

595 (31) Bustin, S. A., Benes, V., Garson, J. A., Hellemans, J., Huggett, J., Kubista, M., Mueller, R., Nolan, T., Pfaffl,
596 M. W., and Shipley, G. L. (2009) The MIQE guidelines: minimum information for publication of quantitative
597 real-time PCR experiments. *Clinical chemistry 55*, 611-622.

598 (32) Schiwy, S., Bräunig, J., Alert, H., Hollert, H., and Keiter, S. H. (2015) A novel contact assay for testing aryl
599 hydrocarbon receptor (AhR)-mediated toxicity of chemicals and whole sediments in zebrafish (Danio rerio)
600 embryos. *Environ Sci Pollut R 22*, 16305-16318.

601 (33) Natto, M. J., Savioli, F., Quashie, N. B., Dardonville, C., Rodenko, B., and de Koning, H. P. (2012)
602 Validation of novel fluorescence assays for the routine screening of drug susceptibilities of Trichomonas
603 vaginalis. *J Antimicrob Chemother 67*, 933-943.

604 (34) Nabb, D. L., Mingoia, R. T., Yang, C. H., and Han, X. (2006) Comparison of basal level metabolic enzyme
605 activities of freshly isolated hepatocytes from rainbow trout (Oncorhynchus mykiss) and rat. *Aquat Toxicol*
606 *80*, 52-59.

607 (35) Escher, B. I., Glauch, L., König, M., Mayer, P., and Schlichting, R. (2019) Baseline Toxicity and Volatility
608 Cutoff in Reporter Gene Assays Used for High-Throughput Screening. *Chemical Research in Toxicology 32*,
609 1646-1655.

610 (36) Fischer, F. C., Cirpka, O. A., Goss, K. U., Henneberger, L., and Escher, B. I. (2018) Application of
611 Experimental Polystyrene Partition Constants and Diffusion Coefficients to Predict the Sorption of Neutral
612 Organic Chemicals to Multiwell Plates in in Vivo and in Vitro Bioassays. *Environ Sci Technol 52*, 13511-
613 13522.

614 (37) Whitlock, J. P. (1999) Induction of cytochrome P4501A1. *Annu Rev Pharmacol 39*, 103-125.

615 (38) Shen, Y., Li, Y., Ye, F., Wang, F., Lu, W., and Xie, X. (2010) Identification of suitable reference genes for
616 measurement of gene expression in human cervical tissues. *Analytical biochemistry 405*, 224-229.

617 (39) Hafner, A., Bulyk, M. L., Jambhekar, A., and Lahav, G. (2019) The multiple mechanisms that regulate p53
618 activity and cell fate. *Nature reviews. Molecular cell biology 20*, 199-210.

619 (40) Jiang, Y. Z., Wang, K., Fang, R., and Zheng, J. (2010) Expression of aryl hydrocarbon receptor in human
620 placentas and fetal tissues. *J Histochem Cytochem 58*, 679-685.

621 (41) Indra, R., Moserova, M., Kroftova, N., Sulc, M., Martinkova, M., Adam, V., Eckschlager, T., Kizek, R., Arlt,
622 V. M., and Stiborova, M. (2014) Modulation of human cytochrome P450 1A1-mediated oxidation of benzo
623 [a] pyrene by NADPH: cytochrome P450 oxidoreductase and cytochrome b5. *Neuro Endocrinol. Lett 35*,
624 105-113.

625 (42) Thakker, D. R., Yagi, H., Lu, A. Y., Levin, W., and Conney, A. H. (1976) Metabolism of benzo[a]pyrene:
626 conversion of (+/-)-trans-7,8-dihydroxy-7,8-dihydrobenzo[a]pyrene to highly mutagenic 7,8-diol-9,10-
627 epoxides. *Proc Natl Acad Sci U S A 73*, 3381-3385.

628 (43) Lind, C., Vadi, H., and Ernster, L. (1978) Metabolism of benzo(a)pyrene-3,6-quinone and 3-
629 hydroxybenzo(a)pyrene in liver microsomes from 3-methylcholanthrene-treated rats. A possible role of DT-
630 diaphorase in the formation of glucuronyl conjugates. *Arch Biochem Biophys 190*, 97-108.

631 (44) Fischer, F. C., Henneberger, L., König, M., Bittermann, K., Linden, L., Goss, K.-U., and Escher, B. I. (2017)
632 Modeling Exposure in the Tox21 in Vitro Bioassays. *Chemical Research in Toxicology 30*, 1197-1208.

633 (45) Shafaie, S., Hutter, V., Brown, M. B., Cook, M. T., and Chau, D. Y. S. (2017) Influence of surface geometry
634 on the culture of human cell lines: A comparative study using flat, round-bottom and v-shaped 96 well plates.
635 *Plos One 12*, e0186799-e0186799.

636 (46) Sa-ngiamsuntorn, K., Wongkajornsilp, A., Kasetsinsombat, K., Duangsa-ard, S., Nuntakarn, L.,
637 Borwornpinyo, S., Akarasereenont, P., Limsrichamrern, S., and Hongeng, S. (2011) Upregulation of CYP
638 450s expression of immortalized hepatocyte-like cells derived from mesenchymal stem cells by enzyme
639 inducers. *BMC Biotechnology 11*, 89.

640 (47) Franklin, M. R. (1972) Inhibition of Hepatic Oxidative Xenobiotic Metabolism by Piperonyl Butoxide.
641 *Biochem Pharmacol 21*, 3287-+.

642 (48) Wambaugh, J. F., Hughes, M. F., Ring, C. L., MacMillan, D. K., Ford, J., Fennell, T. R., Black, S. R., Snyder,
643 R. W., Sipes, N. S., Wetmore, B. A., Westerhout, J., Setzer, R. W., Pearce, R. G., Simmons, J. E., and
644 Thomas, R. S. (2018) Evaluating In Vitro-In Vivo Extrapolation of Toxicokinetics. *Toxicol Sci 163*, 152-
645 169.

646 (49) Wetmore, B. A. (2015) Quantitative in vitro-to-in vivo extrapolation in a high-throughput environment.
647 *Toxicology 332*, 94-101.

648 (50) Wetmore, B. A., Wambaugh, J. F., Ferguson, S. S., Sochaski, M. A., Rotroff, D. M., Freeman, K., Clewell,
649 H. J., III, Dix, D. J., Andersen, M. E., Houck, K. A., Allen, B., Judson, R. S., Singh, R., Kavlock, R. J.,
650 Richard, A. M., and Thomas, R. S. (2012) Integration of Dosimetry, Exposure, and High-Throughput
651 Screening Data in Chemical Toxicity Assessment. *Toxicol Sci 125*, 157-174.

652 (51) Fay, K. A., Fitzsimmons, P. N., Hoffman, A. D., and Nichols, J. W. (2017) Comparison of trout hepatocytes
653 and liver S9 fractions as in vitro models for predicting hepatic clearance in fish. *Environ Toxicol Chem 36*,
654 463-471.

655 (52) Bteich, M., Poulin, P., and Haddad, S. (2019) The potential protein-mediated hepatic uptake: discussion on
656 the molecular interactions between albumin and the hepatocyte cell surface and their implications for the in
657 vitro-to-in vivo extrapolations of hepatic clearance of drugs. *Expert Opin Drug Met 15*, 633-658.